

NASA Technical Memorandum 81942

**(NASA-TM-81942) PREDICTION OF FATIGUE-CRACK
GROWTH UNDER VARIABLE AMPLITUDE AND SPECTRUM
LOADING USING A CLOSURE MODEL (NASA) 38 p
HC A03/MF A01 CSCL 20K**

N81-19486

Unclass

G3/39 41622

**PREDICTION OF FATIGUE-CRACK GROWTH
UNDER VARIABLE-AMPLITUDE AND SPECTRUM
LOADING USING A CLOSURE MODEL**

J. C. Newman, Jr.

January 1981

NASA

National Aeronautics and
Space Administration

Langley Research Center
Hampton, Virginia 23665



PREDICTION OF FATIGUE-CRACK GROWTH UNDER VARIABLE-AMPLITUDE AND
SPECTRUM LOADING USING A CLOSURE MODEL

J. C. Newman, Jr.
NASA Langley Research Center
Hampton, Virginia 23665

ABSTRACT

The present paper is concerned with the application of an existing analytical crack-closure model to study crack growth under various load histories. The model was based on a concept like the Dugdale model, but modified to leave plastically-deformed material in the wake of the advancing crack tip.

The model was used to correlate crack-growth rates under constant-amplitude loading, and to predict crack growth under variable-amplitude and aircraft-spectrum loading on 2219-T851 aluminum alloy sheet material. The predicted crack-growth lives agreed well with experimental data. For 80 crack-growth tests subjected to various load histories, the ratio of predicted-to-experimental lives (N_p/N_T) ranged from 0.5 to 1.8. The mean value of N_p/N_T was 0.97 and the standard deviation was 0.27.

SYMBOLS

C_k	material crack-growth constants ($k = 1,5$)
c	half-length of crack, m
c_f	half-length of final crack, m
c_i	half-length of initial crack, m
c_n	half-length of starter notch, m
d	half-length of crack plus tensile plastic zone, m
F	boundary-correction factor on stress intensity
K_{max}	maximum stress-intensity factor, $MPa - m^{1/2}$
K_F	elastic-plastic fracture toughness, $MPa - m^{1/2}$
m	fracture toughness parameter
N	number of cycles
N_D	number of crack-growth delay cycles
N_P	number of cycles predicted from analysis
N_T	number of cycles from test specimen
R	stress ratio (S_{min}/S_{max})
S	applied stress, MPa
S_{max}	maximum applied stress, MPa
S_{min}	minimum applied stress, MPa
S_0	crack-opening stress, MPa
t	specimen thickness, m
W	specimen width, m
α	constraint factor, $\alpha = 1$ for plane stress and $\alpha = 3$ for plane strain
ΔK	stress-intensity factor range, $MPa - m^{1/2}$
ΔK_{eff}	effective stress-intensity factor range, $MPa - m^{1/2}$

ΔK_o	effective threshold stress-intensity factor range, MPa - m ^{1/2}
ΔK_{th}	threshold stress-intensity factor range, MPa - m ^{1/2}
ΔS_{eff}	effective stress range, MPa
ρ	length of tensile plastic zone, m
ρ_{OL}	plastic-zone size calculated from overload, m
σ_o	flow stress (average between σ_{ys} and σ_u), MPa
σ_{ys}	yield stress (0.2 percent offset), MPa
σ_u	ultimate tensile strength, MPa
ω	length of compressive plastic zone, m

INTRODUCTION

Fatigue cracks remain closed during part of the load cycle under fatigue loading. The crack-closure concept has been used to correlate crack-growth rates under constant-amplitude loading [1,2] and is a significant factor in causing load-interaction effects on crack-growth rates (retardation and acceleration) under variable-amplitude loading. Fatigue-crack closure is caused by residual plastic deformations remaining in the wake of an advancing crack.

The crack-closure phenomenon has been analyzed using two-dimensional, elastic-plastic, finite-element methods [3-6]. The finite-element analyses were shown to be quite accurate, but were very complicated and required large computing facilities. There have also been several attempts to develop simple analytical models of crack closure [3,7-12]. All of these models were based on a concept similar to the Dugdale model [13] or strip-yield model, but modified to leave plastically-deformed material in the wake of the crack. Newman [3], Budiansky and Hutchinson [8], and Fühning and Seeger [10,11] studied only the

crack-closure behavior. But, Dill and Saff [7], Hardrath, Newman, Elber and Poe [9], and Newman [12] used the crack-opening stresses from the models to predict crack growth under spectrum loading.

The purpose of the present paper is to apply an existing analytical crack-closure model [12], which simulates plane-stress and plane-strain conditions, to crack growth under various load histories. The model was based on the Dugdale model [13], but modified to leave plastically-deformed material along the crack surfaces as the crack advances. Plane-stress and plane-strain conditions were simulated by using a "constraint" factor on tensile yielding.

The crack-closure model, developed in reference 12, was for a central crack in a finite-width plate that was subjected to a uniformly applied stress. To calculate Elber's effective stress-intensity factor range [2], crack-opening stresses were calculated from the model under constant-amplitude loading at various applied stress levels and stress ratios. Experimental crack-growth rate data from 2219-T851 aluminum alloy sheet material under constant-amplitude loading [14] were correlated with the effective stress-intensity factor range for a wide range of stress levels and stress ratios. An equation relating crack-growth rate to effective stress-intensity factor range, threshold stress-intensity factor range, and fracture toughness, developed in reference 12, was applied herein over the total range of crack-growth rates. The closure model was then used to predict crack growth in 2219-T851 aluminum alloy sheet material under variable-amplitude and aircraft-spectrum loading [14].

ANALYTICAL CRACK-CLOSURE MODEL

The following section is a brief description of the analytical crack-closure model developed in reference 12.

To calculate crack-closure and crack-opening stresses during crack propagation, the elastic-plastic solution for stresses and displacements in a cracked body must be known. Because there are no closed-form solutions to elastic-plastic cracked bodies, simple approximations must be used. The Dugdale model [13] is one such approximation. The crack-surface displacements, which are used to calculate contact (or closure) stresses under cyclic loading, are influenced by plastic yielding at the crack tip and residual deformations left in the wake of the advancing crack. The applied stress level at which the crack surfaces become fully open (no surface contact) is directly related to contact stresses. This stress is called the "crack-opening stress."

The model was developed for a central crack in a finite-width specimen subjected to uniform applied stress, as shown in figure 1. The model was based on the Dugdale model but modified to leave plastically-deformed material in the wake of the crack. The primary advantage in using this model is that the plastic-zone size and crack-surface displacements are obtained by superposition of two elastic problems: a crack in a finite-width plate subjected to (1) a remote uniform stress, S , or (2) a uniform stress, σ , applied over a segment of the crack surface. The stress-intensity factor and crack-surface displacement equations for these loading conditions are given in reference 12.

Figure 2 shows a schematic of the model at maximum and minimum applied stresses. The model was composed of three regions: (1) a linear elastic region containing a fictitious crack of half-length $c + \rho$, (2) a plastic region of length ρ , and (3) a residual plastic deformation region along the crack surfaces. The physical crack is of half-length c . The compressive plastic zone is ω . Region 1 was treated as an elastic continuum, and the crack-surface displacements under various loading conditions are given in reference 12.

Regions 2 and 3 were composed of rigid-perfectly plastic (constant stress) bar elements with a flow stress, σ_0 , which is the average between the yield stress, σ_{ys} , and the ultimate tensile strength, σ_u . The shaded regions in figure 2(a) and 2(b) indicate material which is in a plastic state. At any applied stress level, the bar elements are either intact (in the plastic zone) or broken (residual plastic deformation). The broken elements carry compressive loads only, and then only if they are in contact. The elements in contact yield in compression when the contact stress reaches $-\sigma_0$. Those elements that are not in contact do not effect the calculation of crack-surface displacements. To account for the effects of state-of-stress on plastic-zone size a constraint factor α was used to elevate the tensile flow stress for the intact elements in the plastic zone. The effective flow stress $\alpha\sigma_0$ under simulated plane-stress conditions was σ_0 and under simulated plane-strain conditions was $3\sigma_0$. The constraint factor is a lower bound for plane stress and an approximate upper bound for plane strain. These constraint factors were verified using elastic-plastic finite-element analyses of cracked bodies under plane stress [6] and plane-strain conditions. The procedure used to establish the constraint factor (α) used herein is discussed later.

The analytical crack-closure model, discussed in detail in reference 12, was used to calculate crack-opening stresses, S_0 , as a function of crack length and load history. In turn, the crack-opening stress was used to calculate the effective stress-intensity factor range, as proposed by Elber, and, consequently, the crack-growth rates.

FATIGUE-CRACK GROWTH RATE EQUATION

The crack-growth equation proposed by Elber [2] states that the crack-growth rate is a power function of the effective stress-intensity factor range

only. Later, Hardrath, Newman, Elber, and Poe [9] showed that the power law was inadequate at high growth rates approaching fracture. The results presented in reference 12 showed that it was also inadequate at low growth rates approaching threshold. To account for these effects, the power law was modified in reference 12 to

$$\frac{dc}{dN} = C_1 \Delta K_{\text{eff}}^{C_2} \frac{1 - \left(\frac{\Delta K_o}{\Delta K_{\text{eff}}} \right)^2}{1 - \left(\frac{K_{\text{max}}}{C_5} \right)^2} \quad (1)$$

where

$$\Delta K_o = C_3 \left(1 + C_4 \frac{S_o}{S_{\text{max}}} \right) \quad (2)$$

$$K_{\text{max}} = S_{\text{max}} \sqrt{\pi c} F \quad (3)$$

and

$$\Delta K_{\text{eff}} = (S_{\text{max}} - S_o) \sqrt{\pi c} F \quad (4)$$

The crack-opening stresses, S_o , were calculated from the analytical closure model. Equation (1) gives the "sigmoidal" shape commonly observed when fatigue crack-growth rate data is plotted against stress-intensity factor range. In the intermediate range of crack-growth rates, equation (1) is basically Elber's proposed power law, $C_1 \Delta K_{\text{eff}}^{C_2}$. The constants C_1 to C_5 were determined to best fit experimental data under constant-amplitude loading.

The coefficients C_3 and C_4 were determined from threshold data on the 2219-T851 aluminum alloy sheet material from reference [15]. The effective

threshold stress-intensity factor range, ΔK_0 , was determined from the threshold stress-intensity factor range, ΔK_{th} , as

$$\Delta K_0 = U \Delta K_{th} = \frac{1 - \frac{S_0}{S_{max}}}{1 - R} \Delta K_{th} \quad (5)$$

The coefficient C_5 is the elastic stress-intensity factor at failure or cyclic fracture toughness. The coefficient C_5 was chosen to be $77 \text{ MPa} - \text{m}^{1/2}$ ($70 \text{ ksi} - \text{in}^{1/2}$) on the basis of the crack-growth tests in reference [14]. (See ref. 12.)

The coefficients C_1 and C_2 were found from constant-amplitude rate data [14], after C_3 , C_4 , and C_5 were determined, by using a least-squares regression analysis. The constant-amplitude correlations were made using S_0 values computed from the model with various constraint factors. It was found that an α of about 1.9 would give a good correlation under constant-amplitude loading. The procedure used to obtain α will be discussed later. A summary of the coefficients used to correlate the constant-amplitude data with $\alpha = 1.9$ are as follows:

$$\left. \begin{aligned} C_1 &= 2.486 \times 10^{-10} \quad (.314 \times 10^{-8}) \\ C_2 &= 3.115 \\ C_3 &= 2.97 \text{ MPa} - \text{m}^{1/2} \quad (2.7 \text{ ksi} - \text{in}^{1/2}) \\ C_4 &= 0.8 \\ C_5 &= 77 \text{ MPa} - \text{m}^{1/2} \quad (70 \text{ ksi} - \text{in}^{1/2}) \end{aligned} \right\} \quad (6)$$

When SI units are used, ΔK_{eff} and K_{max} are given in $\text{MPa} - \text{m}^{1/2}$ and dc/dN is given in m/cycle . When U.S. Customary units are used, ΔK_{eff} and K_{max} are given in $\text{ksi} - \text{in}^{1/2}$ and dc/dN is given in $\text{in.}/\text{cycle}$.

Figure 3 shows a plot of ΔK against dc/dN for several R ratios for 2219-T851 aluminum alloy sheet material to illustrate the sigmoidal shape of equation (1). The experimental data were obtained from reference [15] and the curves were calculated from equation (1). The $R = -1$ data were obtained from a small center-crack tension specimen ($W = 76.2 \text{ mm}$) and the other data were obtained from small compact specimens ($W = 50.8 \text{ mm}$). The crack-growth coefficients (C_1 , C_2 , C_3 , and C_4) used to calculate the curves were identical to those shown in equations (6). However, the coefficient C_5 for the small compact specimens was $38.5 \text{ MPa} - \text{m}^{1/2}$ and for the small center-crack specimen was $55 \text{ MPa} - \text{m}^{1/2}$. The coefficients (C_5) were calculated from the Two-Parameter Fracture Criterion [16] using $K_F = 550 \text{ MPa} - \text{m}^{1/2}$ and $m = 1$. These values of K_F and m were obtained from the final crack lengths and maximum stress levels used in the constant-amplitude tests from reference [14]. (See ref. 12.) The crack-growth rate curves in figure 3 are in good agreement with the experimental data.

APPLICATION OF THE CRACK-CLOSURE MODEL AND RATE EQUATION

The analytical crack-closure model [12] and crack-growth program (FAST - Fatigue Crack Growth Analysis of Structures) was applied to constant-amplitude, variable-amplitude and aircraft-spectrum loading on 2219-T851 aluminum alloy sheet material.

Under constant-amplitude loading, the model was exercised under simulated plane stress, plane strain, and conditions between these limits. The particular constraint factor (α) used herein, to approximate the state-of-stress, was

obtained from the constant-amplitude crack-growth rate data. The crack-growth rate equation (eq. (1)) was also determined from the constant-amplitude data.

The same constraint factor was also used to predict crack growth under variable-amplitude and aircraft-spectrum loading. The crack-opening stresses were calculated from the model as a function of crack length and load history, and the crack-growth rates were predicted from equation (1). The predicted crack-growth lives are compared with experimental data in the following sections.

CONSTANT-AMPLITUDE LOADING

Crack-opening stresses.- Reference 12 showed that the calculated crack-opening stresses under constant-amplitude loading were independent of the constraint factor for stress ratios (R) greater than about 0.7 and were equal to the minimum applied stress. Thus, ΔK_{eff} is equal to ΔK for $R \geq 0.7$. Using crack-growth rate data from references 14 and 15 for $R \geq 0.7$, the crack-growth constants C_1 and C_2 were determined to best fit the high R value data only. Basically, this crack-growth rate equation (eq. (1)) depicts the relation between ΔK_{eff} and crack-growth rate. If ΔK_{eff} and dc/dN are unique, then the crack-growth rates for tests at R ratio less than 0.7 should indicate the experimental ΔK_{eff} and, consequently, the experimental value of S_0 . This value of S_0 is referred to as the "semi-empirical" crack-opening stress. For each test, the semi-empirical S_0 value was assumed to be constant and was determined from a least-squares regression analysis. These crack-opening stresses, normalized by the maximum applied stress, are shown in figure 4 as a function of the R ratio (symbols). The open symbols and the solid circular symbol are results from center-crack tension (CCT) specimens [14,15]. The solid triangular symbols are results from compact specimens [15]. These

results indicate S_0 values that correlate crack-growth rate data at various R ratios with the results at $R \geq 0.7$. The dashed line indicates where S_0 is equal to S_{min} or where ΔK_{eff} is equal to ΔK .

For R ratios less than 0.7, the calculated crack-opening stresses from the closure model are a function of the constraint factor. The semi-empirical results at $R = 0$ were used to estimate the constraint factor. A value of 1.9 was found to give good agreement between the calculated and semi-empirical values. The solid curves show calculations from the closure model with $\alpha = 1.9$ for various applied stress levels. The overall agreement between the calculated and semi-empirical values was considered reasonable.

Crack-growth calculations.- The crack-closure model with $\alpha = 1.9$ was used to calculate the crack-growth lives from the initial crack length c_i to the final crack length c_f for the constant-amplitude tests [14] used in figure 4. The ratio of predicted-to-experimental lives (N_p/N_T) ranged from 0.6 to 1.8. The mean value of N_p/N_T was 1.01 and the standard deviation was 0.32. These calculations were considered reasonable, in view of the scatter that occurs in fatigue-crack growth rate tests.

VARIABLE-AMPLITUDE LOADING

Crack-opening stresses.- The closure model ($\alpha = 1.9$) was used to study the crack-opening stresses under various load histories. The calculated crack-opening stresses under single-spike and two-level loading are shown in figure 5 as a function of crack length. Under spike loading, S_0 takes a sudden drop when the crack-tip region blunts due to the spike loading. As the crack grows into the overload plastic zone (ρ_{OL}), the S_0 values rapidly increase until they reach a maximum value at about one-half of ρ_{OL} . This is the point of minimum crack-growth rate. The S_0 values then drop and approach the

stabilized crack-opening stress (dashed line) for the low-level constant-amplitude loading. The retardation effects (S_0 greater than dashed line) are nearly eliminated when the crack has grown about one overload plastic-zone size. In contrast, under two-level loading the high load was applied from the initial crack length ($c_i = 3$ mm) for about 2500 cycles. Again, the S_0 values rapidly increase as the crack grows into the overload plastic zone, but they reach higher values than those occurring under the single-spike loading. Thus, retardation effects are much stronger after multi-overloads than after single-spike loading.

The calculated crack-opening stresses under compression-tension and tension-compression spike loading are shown in figure 6 as a function of crack length. The horizontal line is the crack-opening stress for the high R ratio (0.5) constant-amplitude loading. Under compression-tension spike loading, the "compressive underload" (single downward load excursion) had no influence on the subsequent S_0 values. But the tensile overload caused the S_0 values to drop immediately, then rapidly rise above those from the steady state constant-amplitude loading (dashed line) for about one overload plastic-zone size. If the compressive underload is applied immediately after the tensile overload, the S_0 values are considerably lower than those from the compression-tension spike loading. Thus, the compressive underload after the spike eliminates some of the retardation effects due to the tensile overload. A larger compressive underload after the spike causes a larger reduction in the S_0 values, but did not completely eliminate the retardation effect due to the tensile overload.

Figure 7 shows the calculated crack-opening stresses during repeated compression-tension spike loading as a function of crack length. The first

load level (i = 1) was applied for 2500 cycles. The compression-tension spike (i = 2) was then applied. These load sequences were repeated until the specimen failed. The dashed line shows the stabilized crack-opening stress (S_{o1}) for level 1 only. The dash-dot line shows the stabilized crack-opening stress if level 2 only was applied. These results show that the interaction between levels 1 and 2 cause S_o values to increase slightly during the compressive underload, drop abruptly during the tensile overload and rapidly increase during the application of the 2500 cycles. Again, the S_o values reach a maximum as the crack grows into the plastic zone caused by the tensile overload. The S_o values would approach S_{o1} if the tensile overload was not repeated.

Crack-growth predictions.- The crack-growth rate, at each load cycle, was computed from equation (1), using the current values of S_{max} , S_{min} , and S_o . Equation (1) predicts retardation (or acceleration) if S_o is larger (or smaller) than the crack-opening stress that would have been produced under constant-amplitude loading at S_{max} and S_{min} . To demonstrate how crack-growth rates were calculated under variable-amplitude loading, an example is given. Figure 8 shows a typical variable-amplitude load history. The growth rate was computed from equation (1) using

$$\Delta K_{eff} = \Delta S_{effk} \sqrt{\pi c} F \quad (7)$$

where ΔS_{effk} is the effective stress range on the k^{th} cycle. The growth increment per cycle is

$$\Delta c_k = \left(\frac{dc}{dN} \right)_k \quad (8)$$

On the first and second tensile load excursion, $S_{\min k}$ to $S_{\max k}$,

$$\Delta S_{\text{eff}k} = S_{\max k} - S_0$$

where $k = 1$ or 2 , respectively. This equation was proposed by Elber [2].

However, on the third tensile load excursion, $S_{\min 3}$ is greater than S_0 , therefore the effective stress range was assumed to be

$$\Delta S_{\text{eff}k} = \left[(S_{\max k} - S_0)^{C_2} - (S_{\min k} - S_0)^{C_2} \right]^{\frac{1}{C_2}} \quad (10)$$

where $k = 3$ and C_2 is the power on the growth law. Thus, the growth increment, $\Delta c_2 + \Delta c_3$, is slightly larger than Δc_1 , if $S_{\max 1} = S_{\max 3}$. The use of equation (10) was necessary because no crack-growth law, when expressed in terms of a power function ($C_2 \neq 1$), would sum to the correct growth increment under variable-amplitude loading. For instance, if the load excursion $S_{\max 2}$ to $S_{\min 3}$ was extremely small, then the sum of growth increments Δc_2 and Δc_3 should be equal to the growth increment Δc_1 . If $S_{\min 3}$ was less than S_0 , then the growth increment Δc_3 should be equal to the growth increment Δc_1 . Equation (10) accounts for these limiting behaviors. Equation (10) is applied only when $S_{\min k}$ is greater than S_0 and only when the current maximum applied stress is higher than the highest maximum stress occurring since a stress excursion crossed S_0 . On the fourth excursion, ΔS_{eff} was, again, computed from equation (9). The effective stress range on the 5th and 7th excursion were, again, computed from equation (10). But on the 6th, 8th, and 9th excursion,

$$\Delta S_{\text{eff}k} = S_{\max k} - S_{\min k} \quad (11)$$

where $k = 6, 8, \text{ or } 9$, respectively. Note that $S_{\max_6} \leq S_{\max_5}$. Equation (11) was also proposed by Elber [2].

Figure 9 shows the effect of the number of overload cycles on predicted crack-growth delay. Crack-growth delay is the additional number of cycles required to grow the crack to failure, following an overload, over the number required to grow the crack to failure under constant-amplitude loading only (level 3). The predicted results (symbols) show that delay or retardation is longer for larger number of overload cycles. These results are in quantitative agreement with experimental observations [17]. Other retardation models account for the effect of the number of overload cycles on crack-growth retardation empirically [18], or do not account for it at all [19,20].

A comparison between experimental and predicted crack-length-against-cycles curves during two-level loading is shown in figure 10. The load sequence is shown in the insert. The high load (level 1) was a factor-of-2 larger than level 2. The predicted results (solid curve) were calculated from equation (1) using the S_0 values computed from the closure model. The maximum computed value of S_0 , during the application of level 2, was about 115 MPa and the minimum crack-growth rate was about 1.4×10^{-7} m/cycle. The predicted life was about one-half of the experimental life (symbols). The dash-dot curve shows the predicted results using no load interaction.

Figure 11 shows a comparison of experimental and predicted crack-length-against-cycles curves for repeated tension-compression and compression-tension spike loading. The load sequences applied are shown in the inserts. The experimental results (symbols) and the predicted results (solid curves) show that the compressive underload applied after the tensile overload causes the crack to grow faster than when the compressive underload occurs before the

tensile overload. Although the predicted results show a stronger effect of the compressive underload than the experimental data, the agreements between the predicted and experimental data are considered good.

A comparison of experimental (symbols) and predicted (solid curve) crack-length-against-cycles curves for a repeated block loading sequence is shown in figure 12. The load sequence is shown in the insert. In contrast to the previous case, fifty cycles of the tensile overload were applied before the compressive underload. The predicted results are in good agreement with the experimental data.

SPECTRUM LOADING

Crack-opening stresses.- The variation of crack-opening stress with crack length for a typical spectrum loading test is shown in figure 13. The half-length of the elox notch (c_n) was 3.2 mm. The specimen was cycled under constant-amplitude loading ($S_{max} = 69$ MPa) at $R = 0$ until the crack grew to a crack half-length (c_i) of 3.8 mm. Next, a typical fighter aircraft spectrum was applied to the specimen. The maximum stress was about 183 MPa and the minimum stress was about -30 MPa. The particular spectrum loads applied are given in reference [14] under test M91. The calculated crack-opening stresses plotted in figure 13 show only a small fraction of the number of values computed from the model. The crack-opening stresses follow a very irregular pattern while the cyclic loads are applied; even so, they tend to oscillate about a mean value.

The use of an "equivalent" crack-opening stress concept would greatly reduce the computer times required to complete a simulated test. The use of an equivalent stress is justified because, at low to medium stress levels, the

crack-opening stresses stabilize under constant-amplitude loading. They also tend to oscillate about a mean value under spectrum loading. The equation for the equivalent crack-opening stress, \bar{S}_0 , was

$$\bar{S}_0 = \frac{\sum (S_0 \Delta c)_k}{\sum \Delta c_k} \quad (12)$$

where the summation was performed over the crack extension increment $c_i + 5 \rho_{\max}$ to $c_i + 10 \rho_{\max}$. The maximum plastic-zone size, ρ_{\max} , was calculated using the maximum stress in the spectrum. (For extremely high stress levels and low R ratios, where S_0 values do not stabilize, the simulated test specimen may fail before the equivalent crack-opening stress routine is activated.) The dashed line in figure 13 shows the calculated equivalent crack-opening stress. The predicted crack-growth life using \bar{S}_0 was 3.5 percent less than the predicted life using S_0 , but the computer time was only about one-half as large (2.6 minutes to 5.6 minutes).

Crack-growth predictions.— In reference 14 crack-growth tests were conducted on center-crack tension specimens subjected to five basic aircraft-type load spectra. Three of the spectra were each applied at three different scale factors (same shape spectrum with different scaling of the stresses), and the other two spectra were each applied at two different scale factors. There were thirteen different spectrum loading tests.

Figure 14 compares predicted and experimental crack-length-against-cycles curves for a typical fighter spectrum. The specimens were subjected to the same spectrum, but with three different scale factors (0.2, 0.3, and 0.4). The predicted results using $\alpha = 1.9$ (solid curves) are in good agreement with the experimental data (symbols). However, for all spectrum tests conducted at a

low-stress level (scale factor = 0.2), the predicted results gave longer lives than the experimental data. At the low-stress level, the plastic-zone sizes are small compared to thickness and plane-strain conditions may prevail. The dashed curve shows calculated results using a constrain factor of 2.7 (plane strain) and the results are in excellent agreement with the experimental data, whereas, at the high-stress level, the predicted results gave shorter lives than the experimental data. At the high-stress level, the plastic-zone sizes are about a factor-of-4 larger than the low-stress level case, and plane-stress conditions may prevail. The dash-dot curve was calculated using an $\alpha = 1.15$. The calculated results are in better agreement with the experimental data than the results with an $\alpha = 1.9$. These results indicate that the constraint factor may vary with stress level and crack length.

COMPARISON OF EXPERIMENTAL AND PREDICTED LIVES

Figure 15 compares experimental (N_T) and predicted (N_p) lives for 18 constant-amplitude load tests, 49 variable-amplitude load tests, and 13 spectrum-load tests. The crack-closure model with $\alpha = 1.9$ was used to predict crack-growth lives from the initial crack length c_i to the final crack length c_f . The ratio of predicted-to-experimental life (N_p/N_T) ranged from 0.5 to 1.8. The mean value of N_p/N_T was 0.97 and the standard deviation was 0.27.

CONCLUDING REMARKS

An existing analytical crack-closure model (FAST) was used to correlate crack-growth rate data under constant-amplitude loading, and to predict crack growth under variable-amplitude and aircraft-spectrum loading. The model was based on the Dugdale model, but modified to leave plastically-deformed material

in the wake of the advancing crack tip. The model was used to calculate the crack-opening stresses as a function of crack length and load history under simulated plane-stress and plane-strain conditions.

A previously developed crack-growth rate equation, in terms of Elber's effective stress-intensity factor range, threshold stress-intensity factor range, and fracture toughness, was used to correlate constant-amplitude rate data. The rate equation gives the "sigmoidal" shape commonly observed when fatigue crack-growth rate data is plotted against stress-intensity factor range. The five crack-growth constants in this equation were determined from constant-amplitude data on 2219-T851 aluminum alloy sheet material. The equation correlated the constant-amplitude data over a wide range of stress ratios and stress levels quite well.

The analytical closure model with a constraint factor of 1.9 and the rate equation were used to predict crack growth under variable-amplitude and aircraft-spectrum loading on the 2219-T851 aluminum alloy material. The proper constraint factor was determined from the constant-amplitude data. The model predicts the effects of load interaction, such as retardation and acceleration. The ratio of predicted-to-experimental crack-growth lives (N_p/N_T) ranged from 0.5 to 1.8 in sixty-two variable-amplitude and spectrum load tests. The mean of N_p/N_T was 0.97 and the standard deviation was 0.27. Thus, the analytical crack-closure model and the proposed crack-growth law predicted crack growth behavior in all tests quite well.

REFERENCES

1. Elber, W.: "Fatigue Crack Closure Under Cyclic Tension." *Engineering Fracture Mechanics*, Vol. 2, No. 1, July 1970, pp. 37-45.
2. Elber, W.: "The Significance of Fatigue Crack Closure." ASTM STP-486, American Society for Testing and Materials, 1971, pp. 230-242.
3. Newman, J. C., Jr.: "Finite-Element Analysis of Fatigue Crack Propagation - Including the Effects of Crack Closure." PhD Thesis, VPI & SU, Blacksburg, VA, May 1974.
4. Newman, J. C., Jr.; and Armen, Harry, Jr.: "Elastic-Plastic Analysis of a Propagating Crack Under Cyclic Loading." *AIAA Journal*, Vol. 13, No. 8, August 1975, pp. 1017-1023.
5. Obji, K.; Ogura, K.; and Ohkubo, Y.: "Cyclic Analysis of a Propagating Crack and Its Correlation with Fatigue Crack Growth." *Engineering Fracture Mechanics J.*, Vol. 7, 1975, pp. 457-464.
6. Newman, J. C., Jr.: "A Finite-Element Analysis of Fatigue-Crack Closure." *Mechanics of Crack Growth*, ASTM STP-490, American Society for Testing and Materials, 1976, pp. 281-301.
7. Dill, H. D.; and Saff, C. R.: "Spectrum Crack Growth Prediction Method Based on Crack Surface Displacement and Contact Analyses." *Fatigue Crack Growth Under Spectrum Loads*, ASTM STP-595, American Society for Testing and Materials, 1976, pp. 306-319.
8. Budiansky, B.; and Hutchinson, J. W.: "Analysis of Closure in Fatigue Crack Growth." Division of Applied Science, DAS M-1, Harvard University, June 1977.
9. Hardrath, H. F.; Newman, J. C., Jr.; Elber, W.; and Poe, C. C., Jr.: "Recent Developments in Analysis of Crack Propagation and Fracture of Practical Materials." *Fracture Mechanics*, edited by N. Perrone, University Press of Virginia, 1978.
10. Föhning, H.; and Seeger, T.: "Dugdale Crack Closure Analysis of Fatigue Cracks Under Constant Amplitude Loading." *Engineering Fracture Mechanics J.*, Vol. 11, 1979, pp. 99-122.
11. Föhning, H.; and Seeger, T.: "Structural Memory of Cracked Components Under Irregular Loading." *Fracture Mechanics*, ASTM STP-677, C. W. Smith, Ed., American Society for Testing and Materials, 1979, pp. 144-167.
12. Newman, J. C., Jr.: "A Crack-Closure Model for Predicting Fatigue-Crack-Growth Under Aircraft Spectrum Loading." *Methods and Models for Predicting Crack Growth Under Random Loading*, ASTM STP-____, J. B. Chang, Ed., American Society for Testing and Materials, 1981, pp. ____-____.

13. Dugdale, D. S.: "Yielding of Steel Sheets Containing Slits." *Journal Mech. Phys. Solids*, Vol. 8, 1960.
14. Chang, J. B.; and Stolpestad, J. H.: "Improved Methods for Predicting Spectrum Loading Effects - Phase I Report." AFFDL-TR-79-3036, Volume II, March 1978.
15. Hudak, S. J.; Saxena, A.; Bucci, R. J.; and Malcolm, R. C.: "Development of Standard Methods of Testing and Analyzing Fatigue Crack Growth Rate Data." AFML-TR-78-40, May 1978.
16. Newman, J. C., Jr.: "Fracture Analysis of Various Cracked Configurations in Sheet and Plate Materials, Properties Related to Fracture Toughness." ASTM STP-605, American Society for Testing and Materials, 1976, pp. 104-123.
17. Hudson, C. M.; and Raju, K. N.: "Investigation of Fatigue-Crack Growth Under Simple Variable-Amplitude Loading." *International Journal of Nondestructive Testing*, Vol. 2, 1970, pp. 189-205.
18. Johnson, W. S.: "Multi-Parameter Yield Zone Model for Predicting Spectrum Crack Growth." *Methods and Models for Predicting Fatigue Crack Growth Under Random Loading*, ASTM STP, J. B. Chang, Ed., American Society for Testing and Materials, 1981.
19. Willenborg, J. D.; Engle, R. M., Jr.; and Wood, H. A.: "A Crack Growth Retardation Model Using Effective Stress Concept." AFFDL-TM-71-1-FBR, Jan. 1971.
20. Chang, J. B.; Engle, R. M.; and Stolpestad, J.: "Fatigue Crack Growth Behavior and Life Predictions for 2219-T851 Aluminum Subjected to Variable-Amplitude Loadings." Presented at the 13th National Symposium on Fracture Mechanics, June 1980.

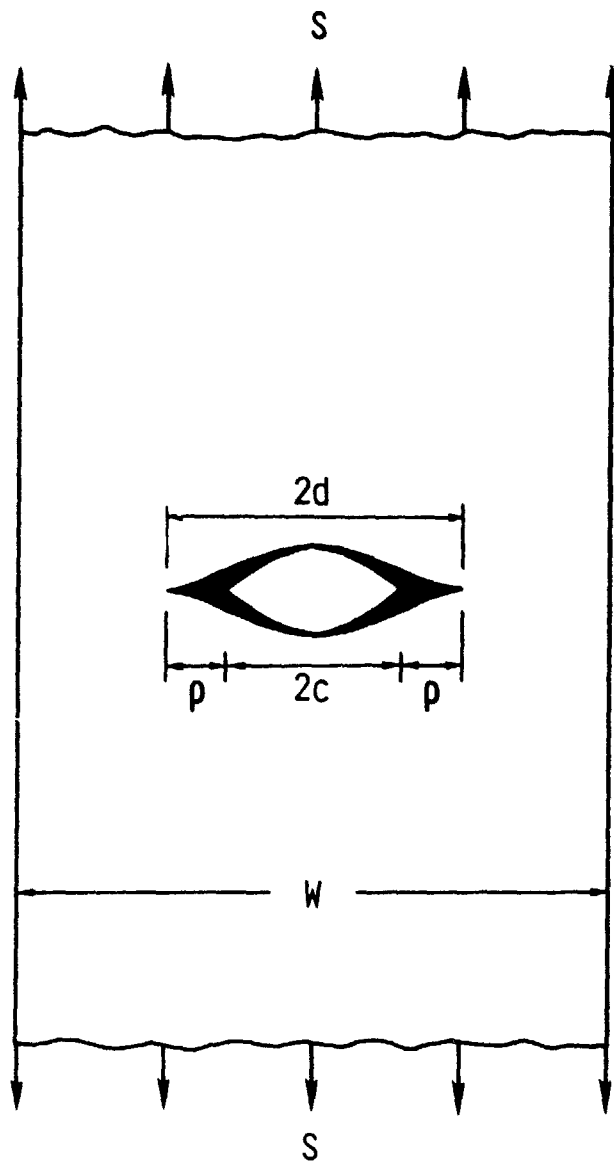
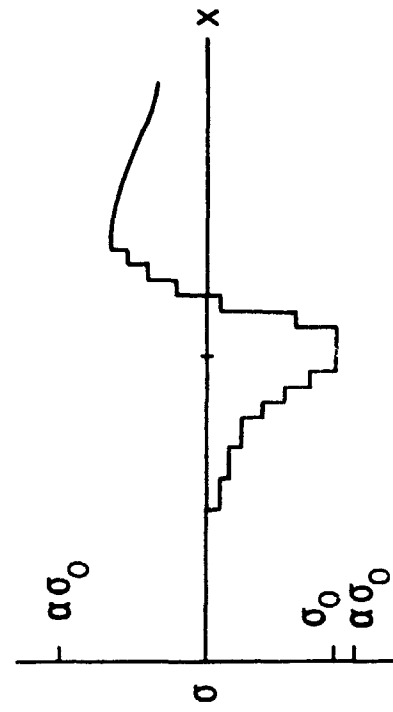
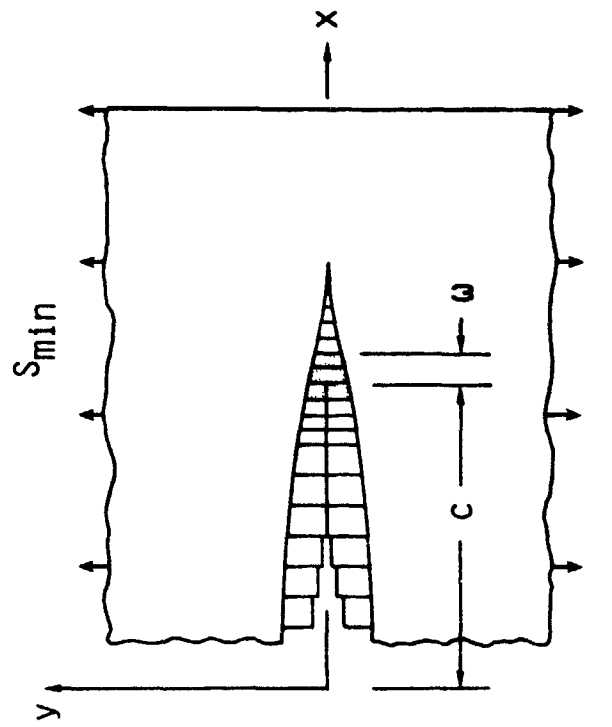
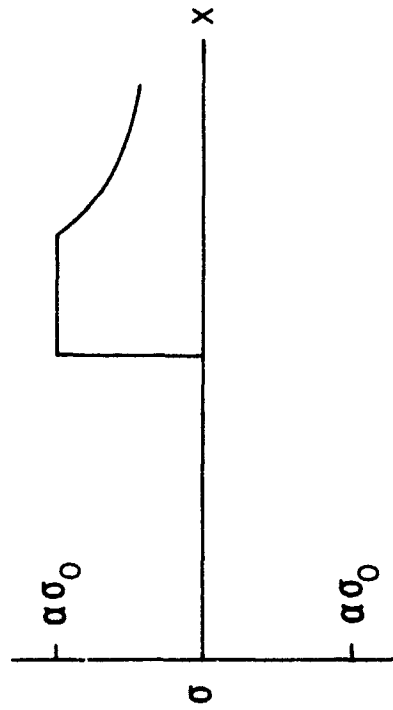
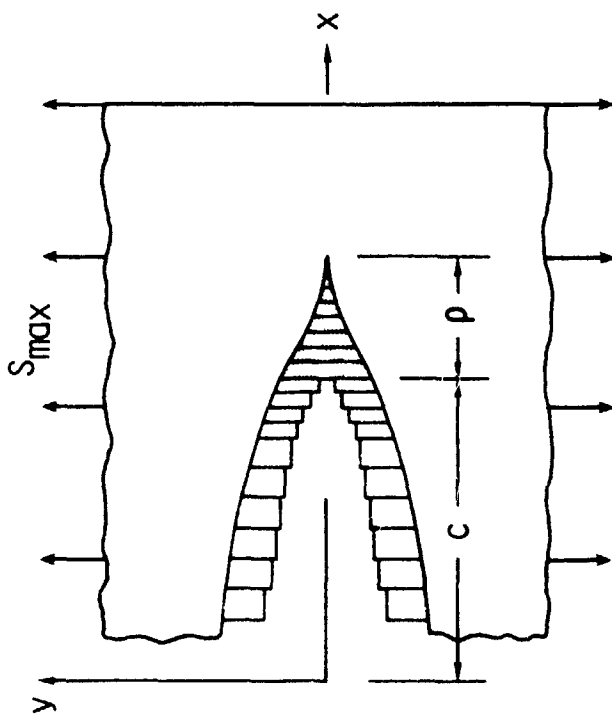


FIG. 1 - Center-crack tension specimen with Dugdale plastic zones and residual plastic deformations.



(a) Maximum stress



(b) Minimum stress

FIG. 2 - Crack-surface displacements and stress distributions along crack line.

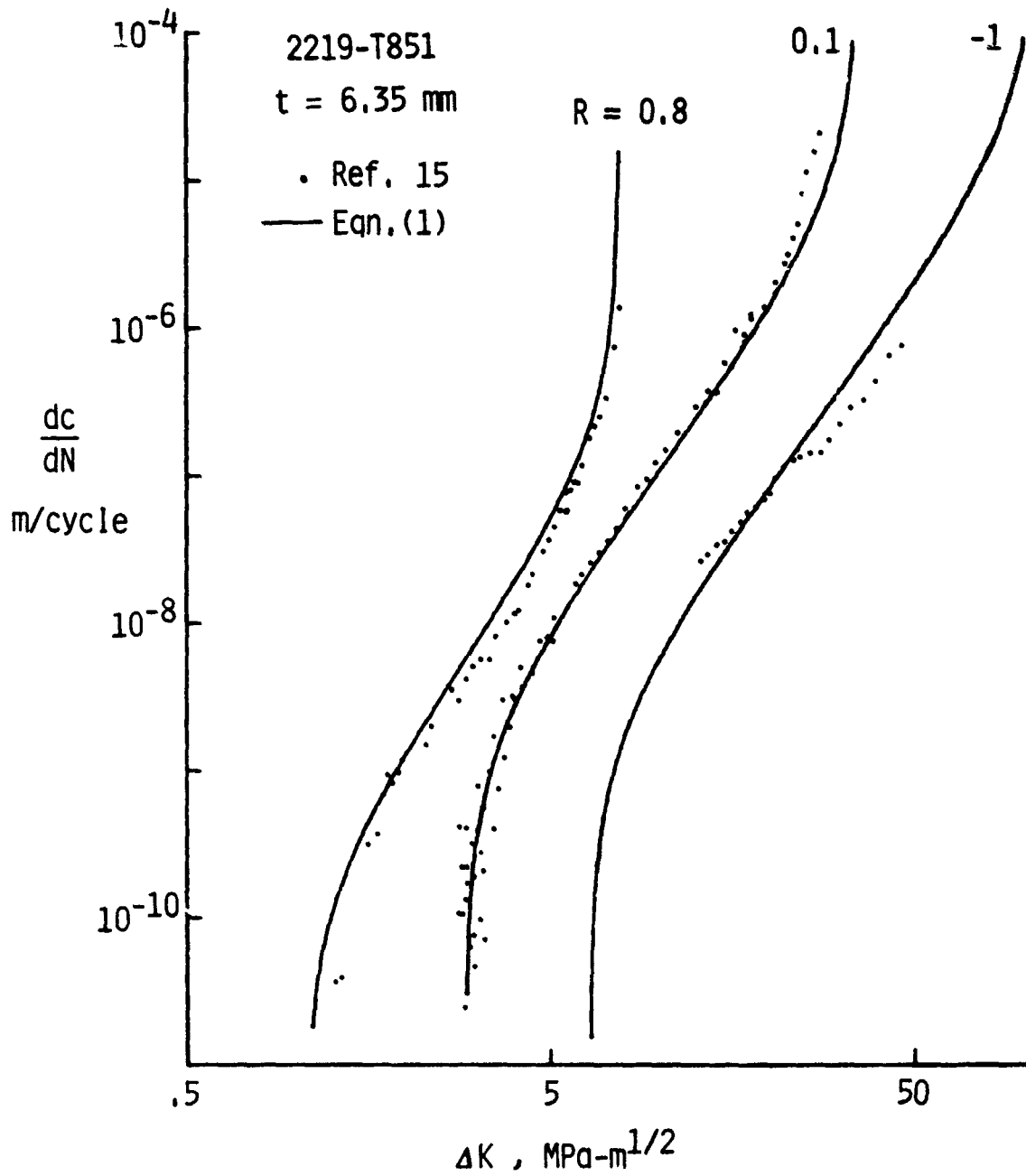


FIG. 3 - Comparison of experimental crack-growth rates and rate equation for 2219-T851 aluminum alloy at various R ratios.

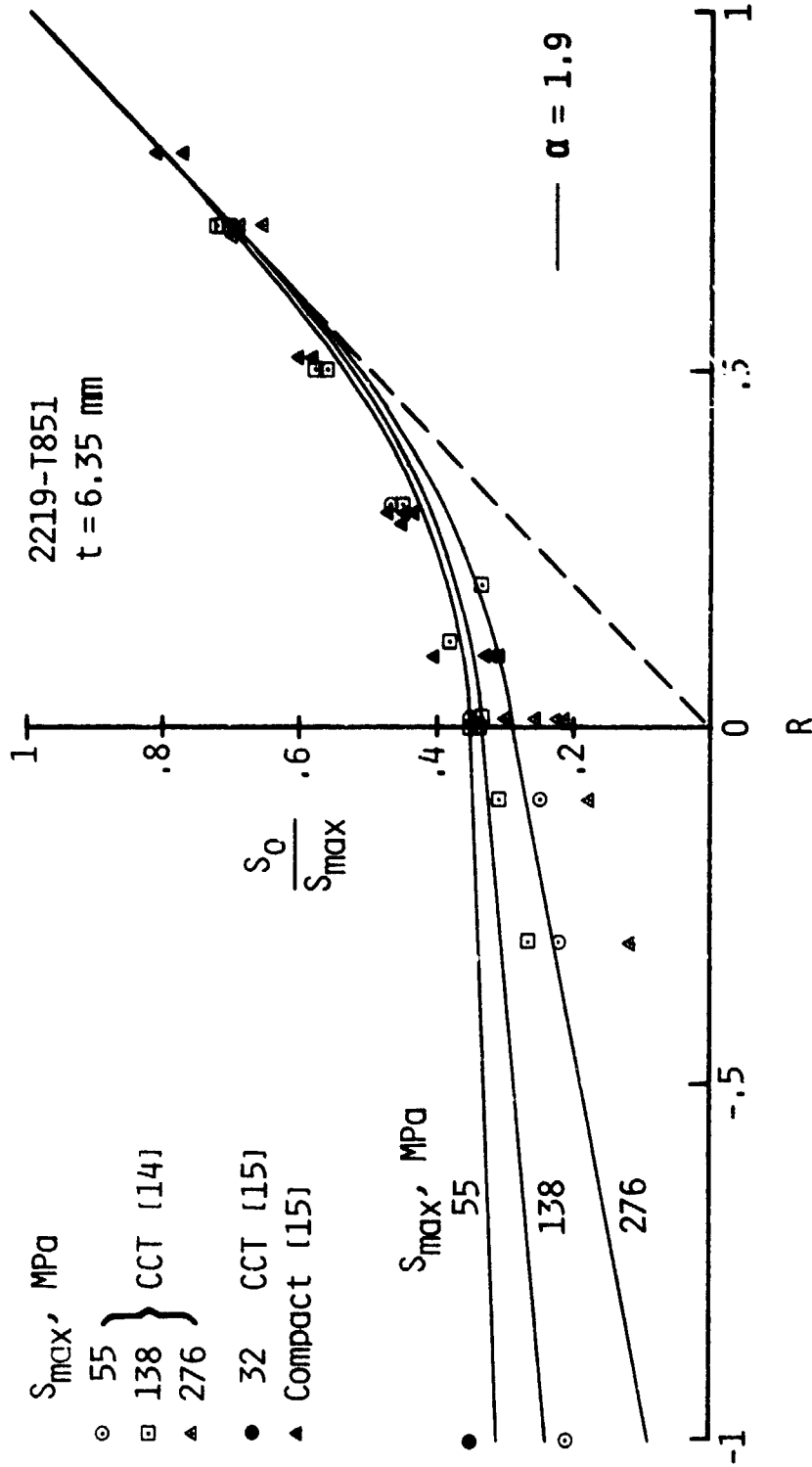


FIG. 4 - Comparison of semi-empirical and calculated crack-opening stresses as functions of stress ratio (R) and stress level (S_{max}).

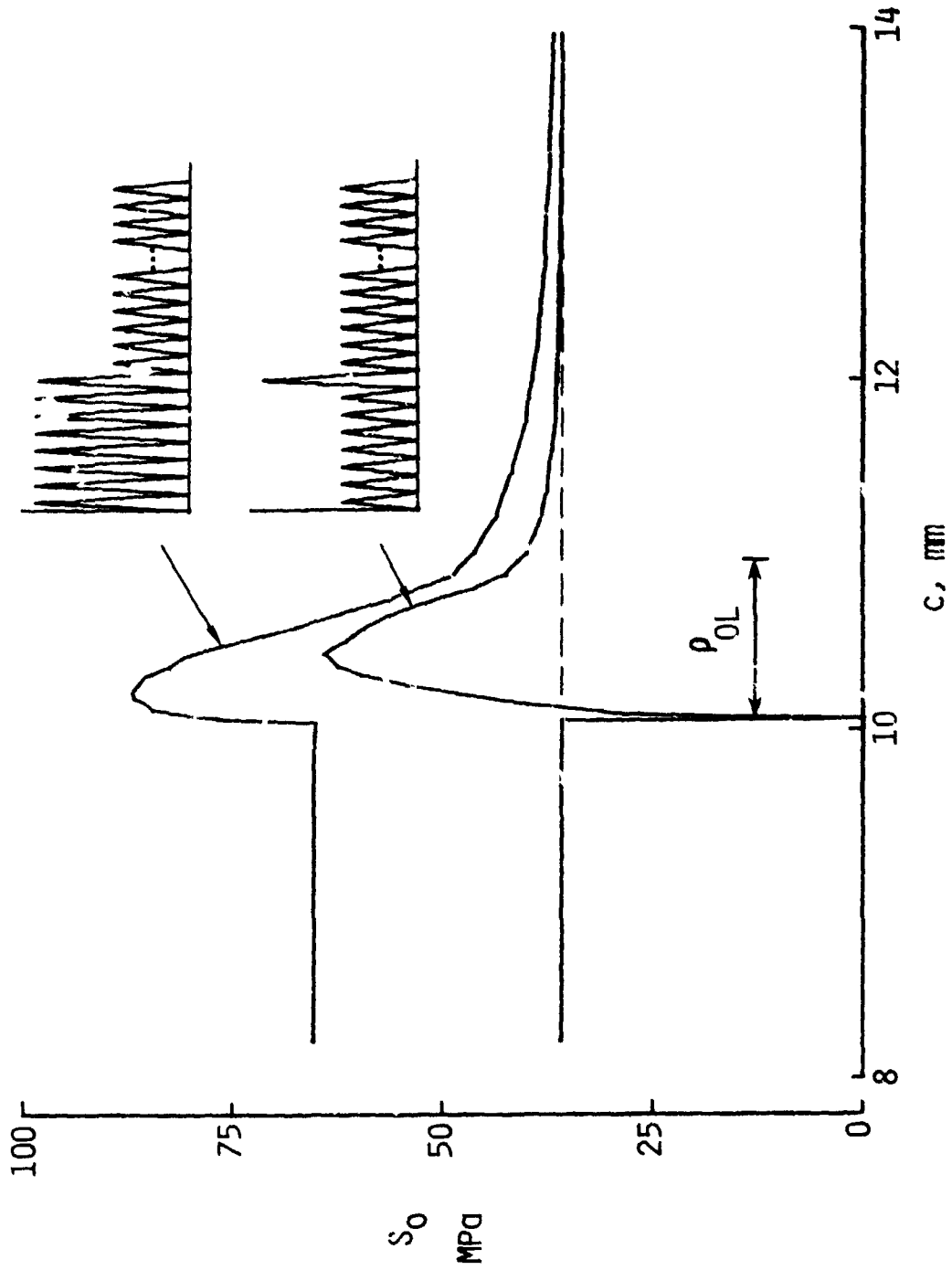


FIG. 5 - Comparison of calculated crack-opening stresses during two-level and single-spike loading as a function of crack length.

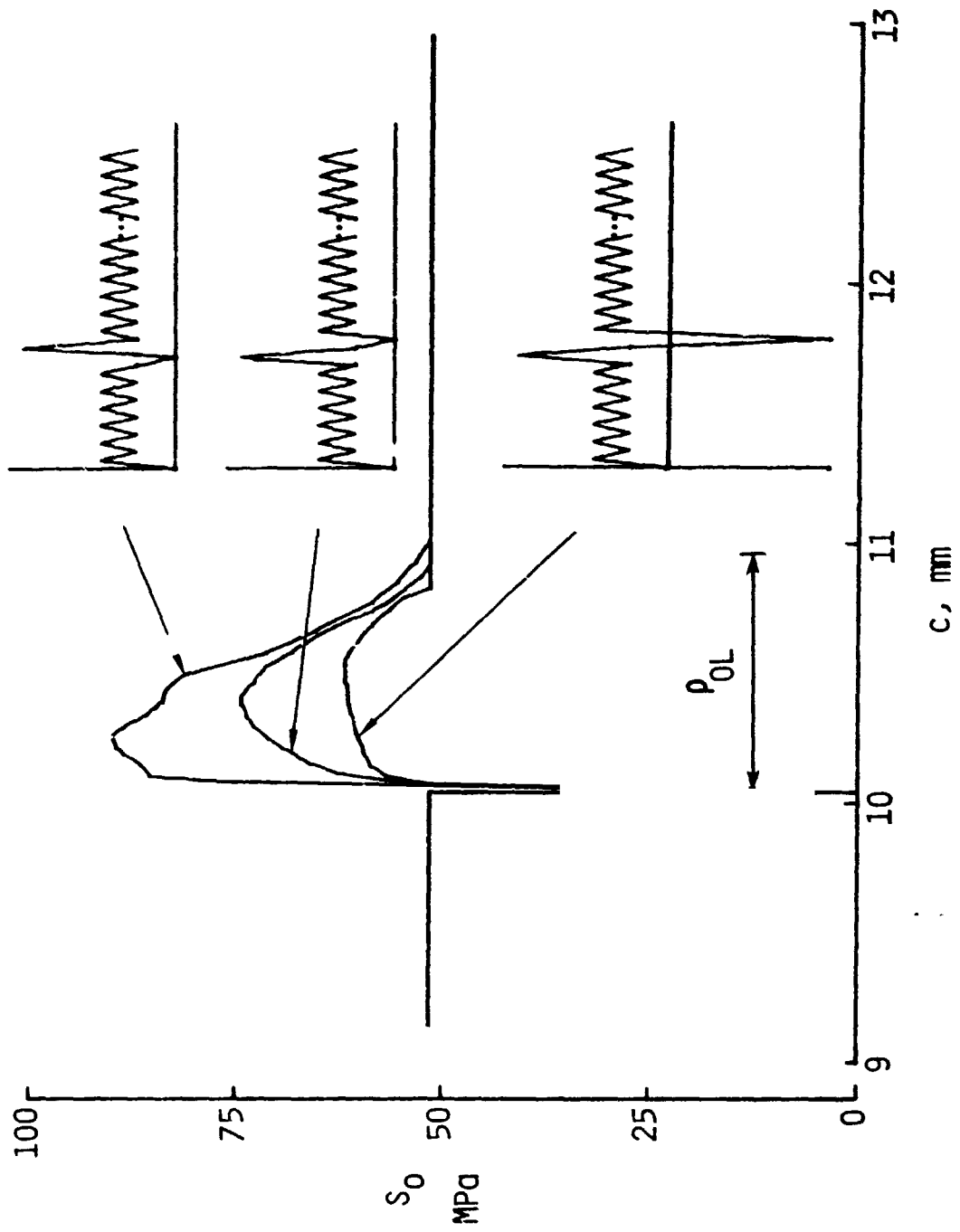


FIG. 6 - Comparison of calculated crack-opening stresses during compression-tension and tension-compression spike loading as a function of crack length.

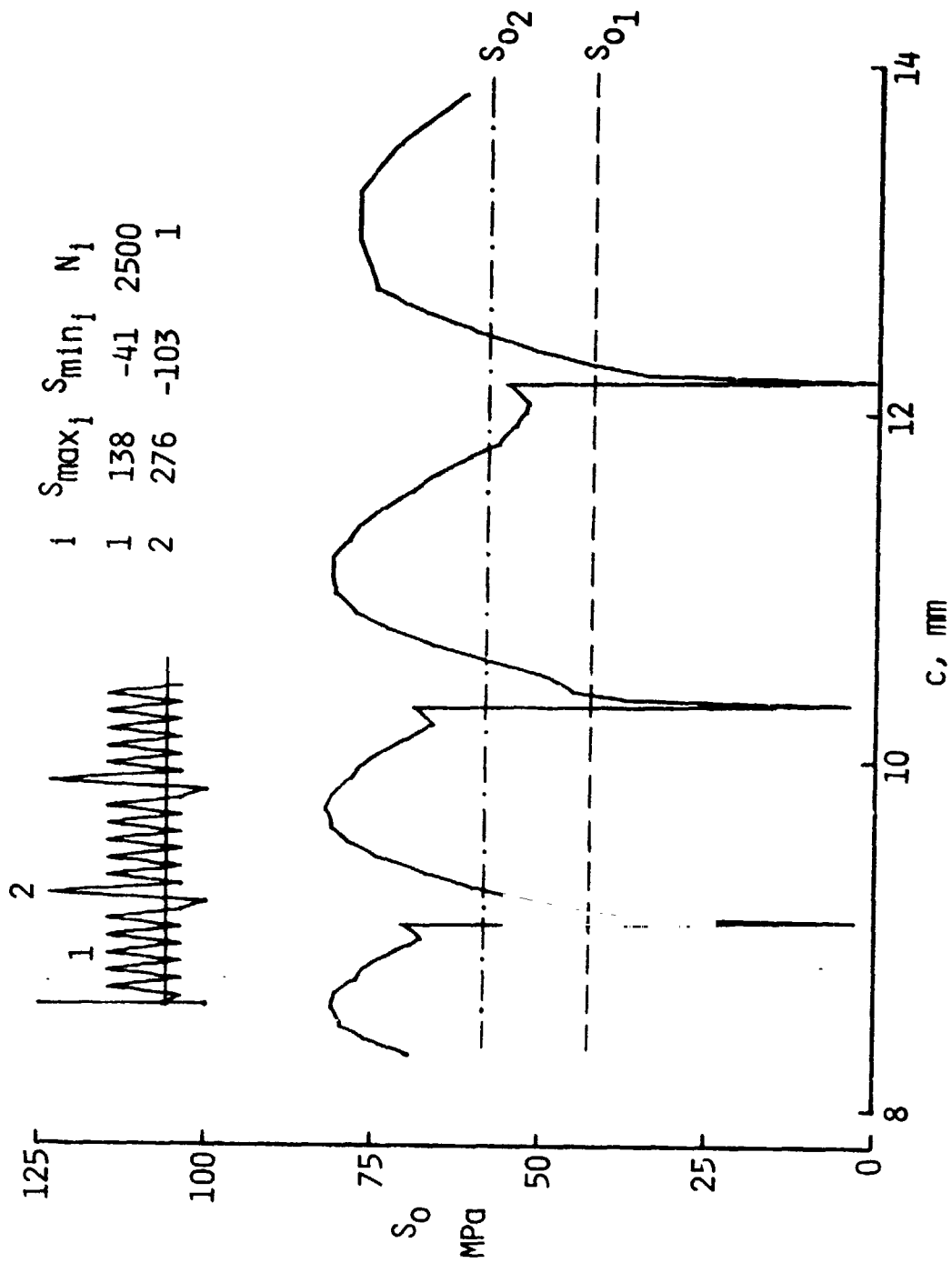


FIG. 7 - Calculated crack-opening stresses during repeated spike loading as a function of crack length.

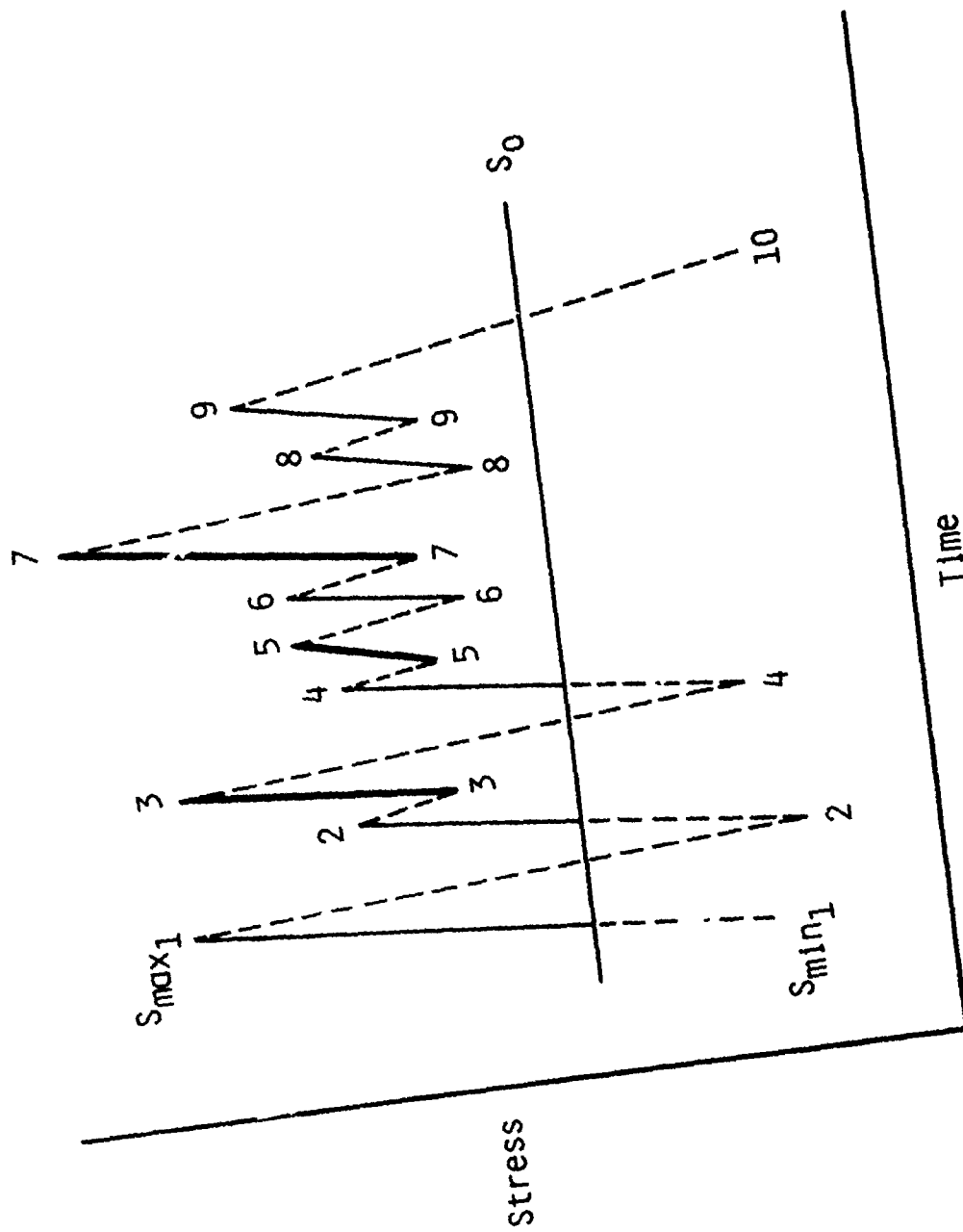


FIG. 8 - Variable-amplitude load history.

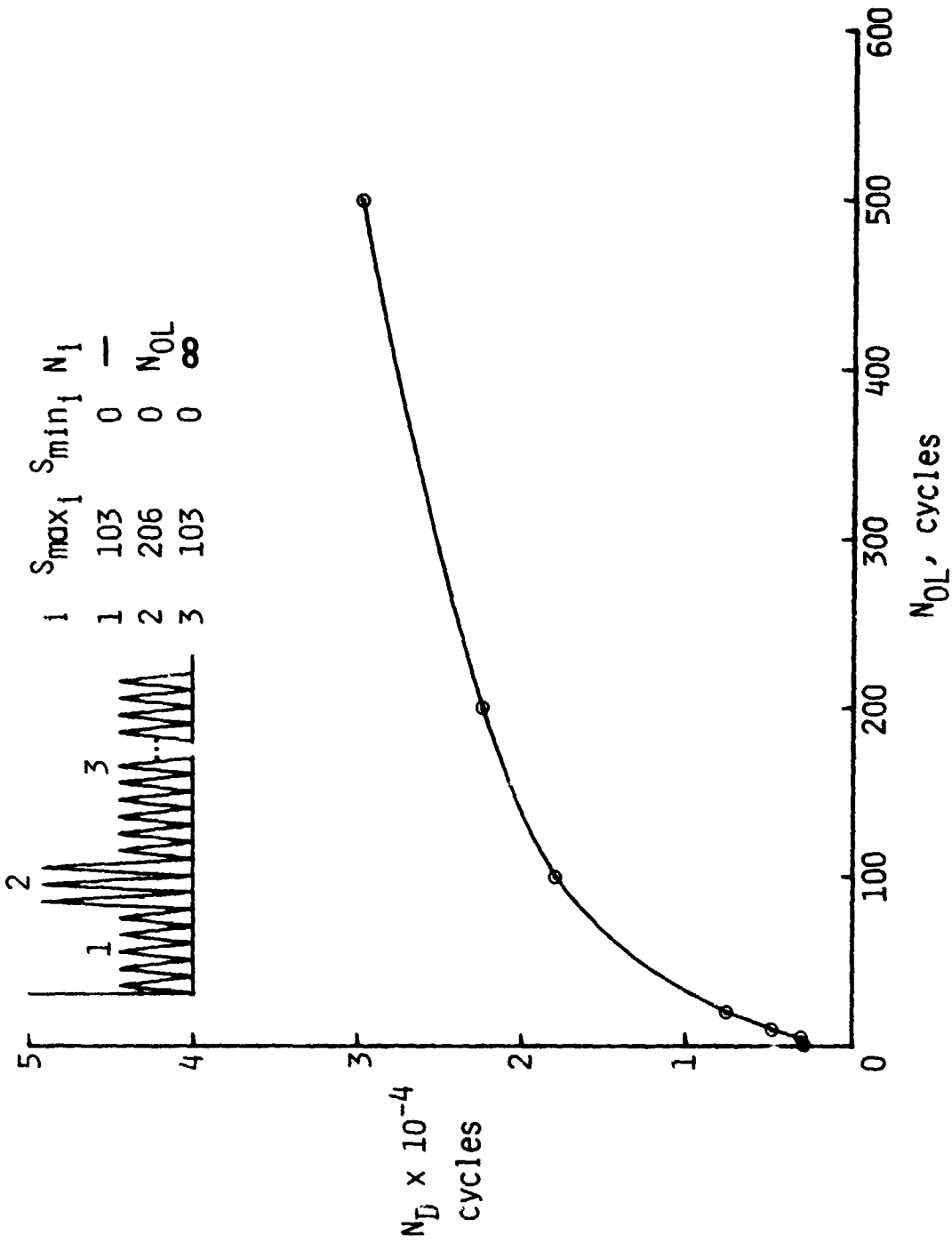


FIG. 9 - Effect of the number of overload cycles on predicted crack-growth delay.

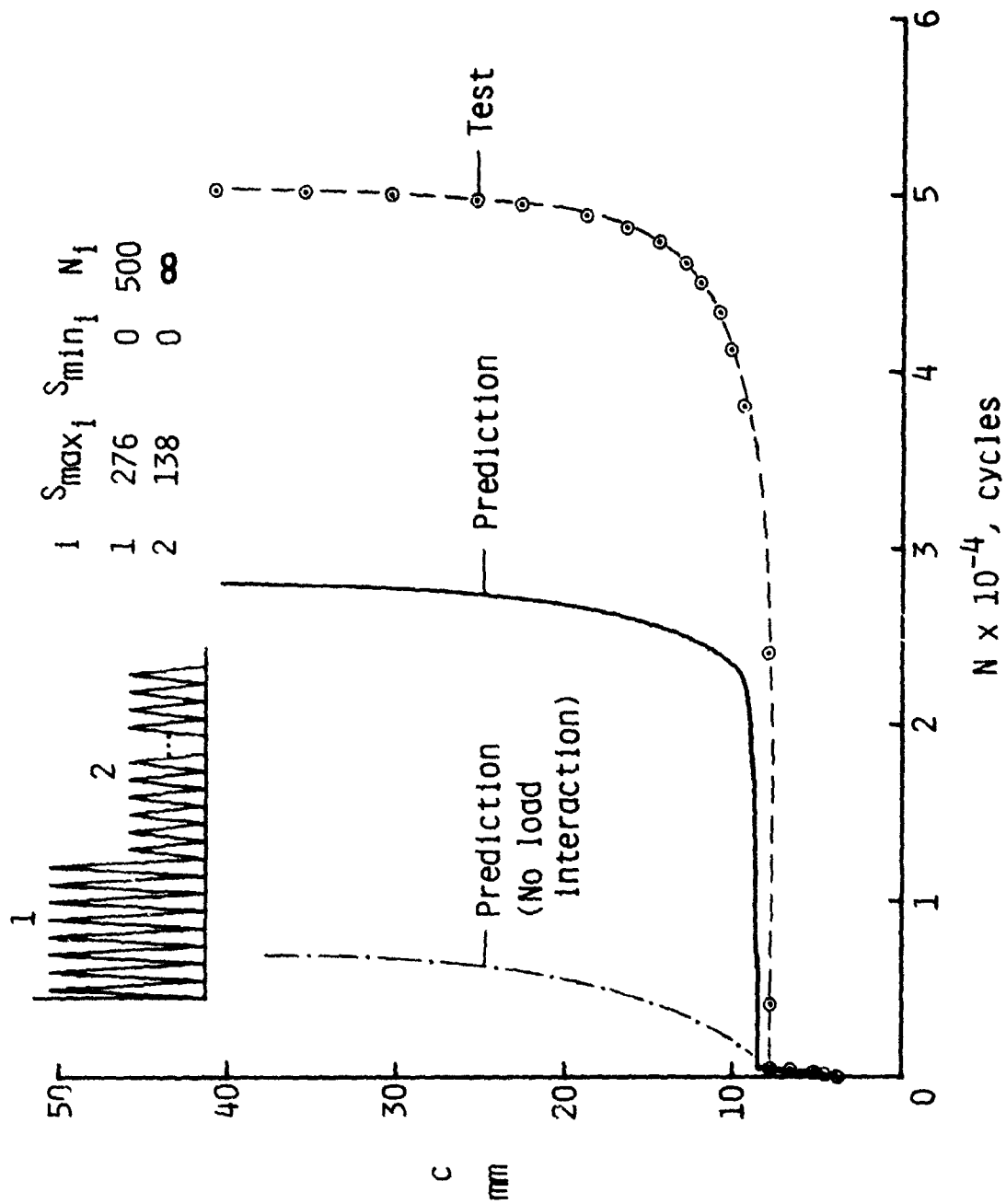


FIG. 10 - Comparison of experimental [14] and predicted crack-length-against-cycles curves during two-level loading.

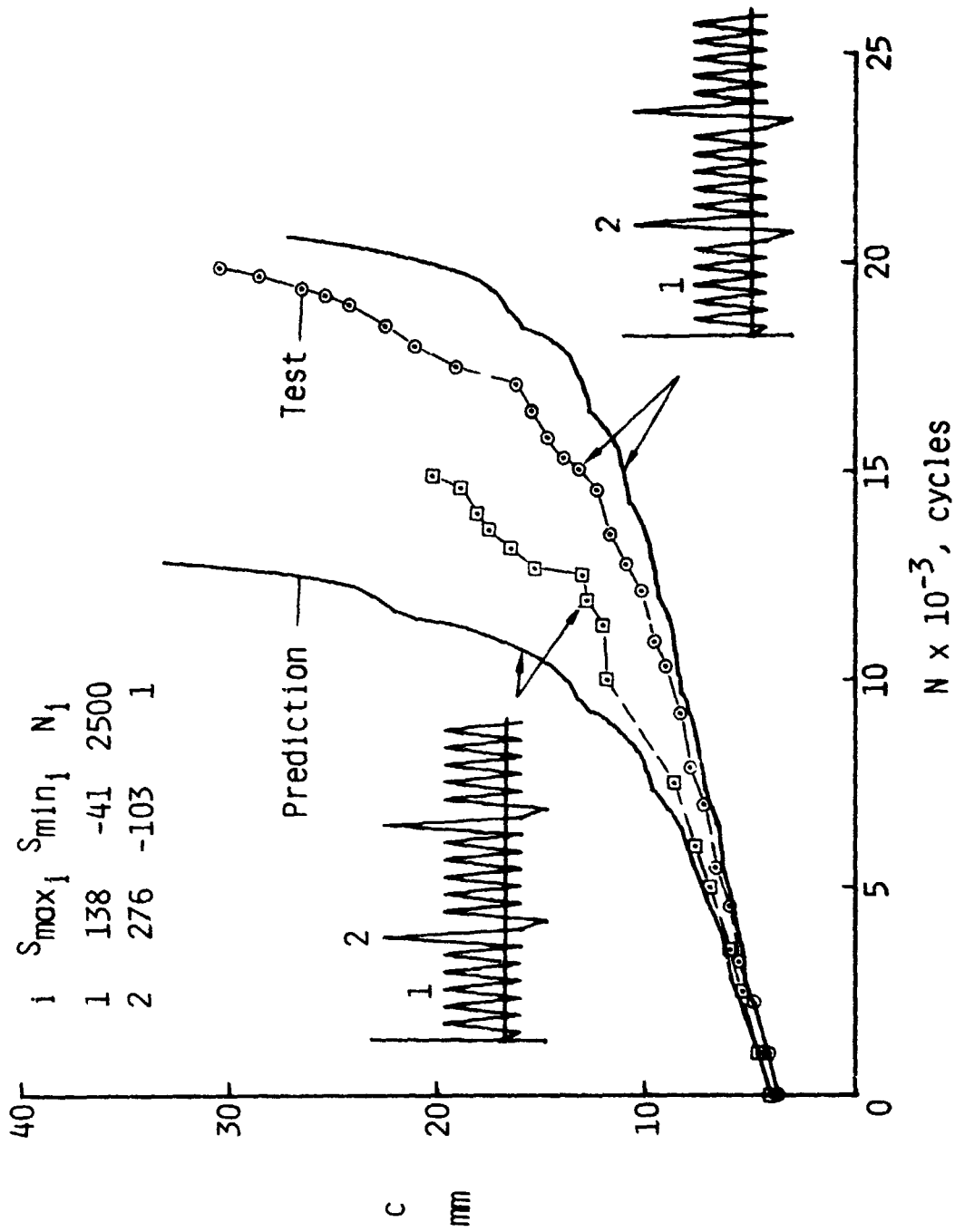


FIG. 11 - Comparison of experimental [14] and predicted crack-length-against-cycles curves during repeated tension-compression and compression-tension spike loading.

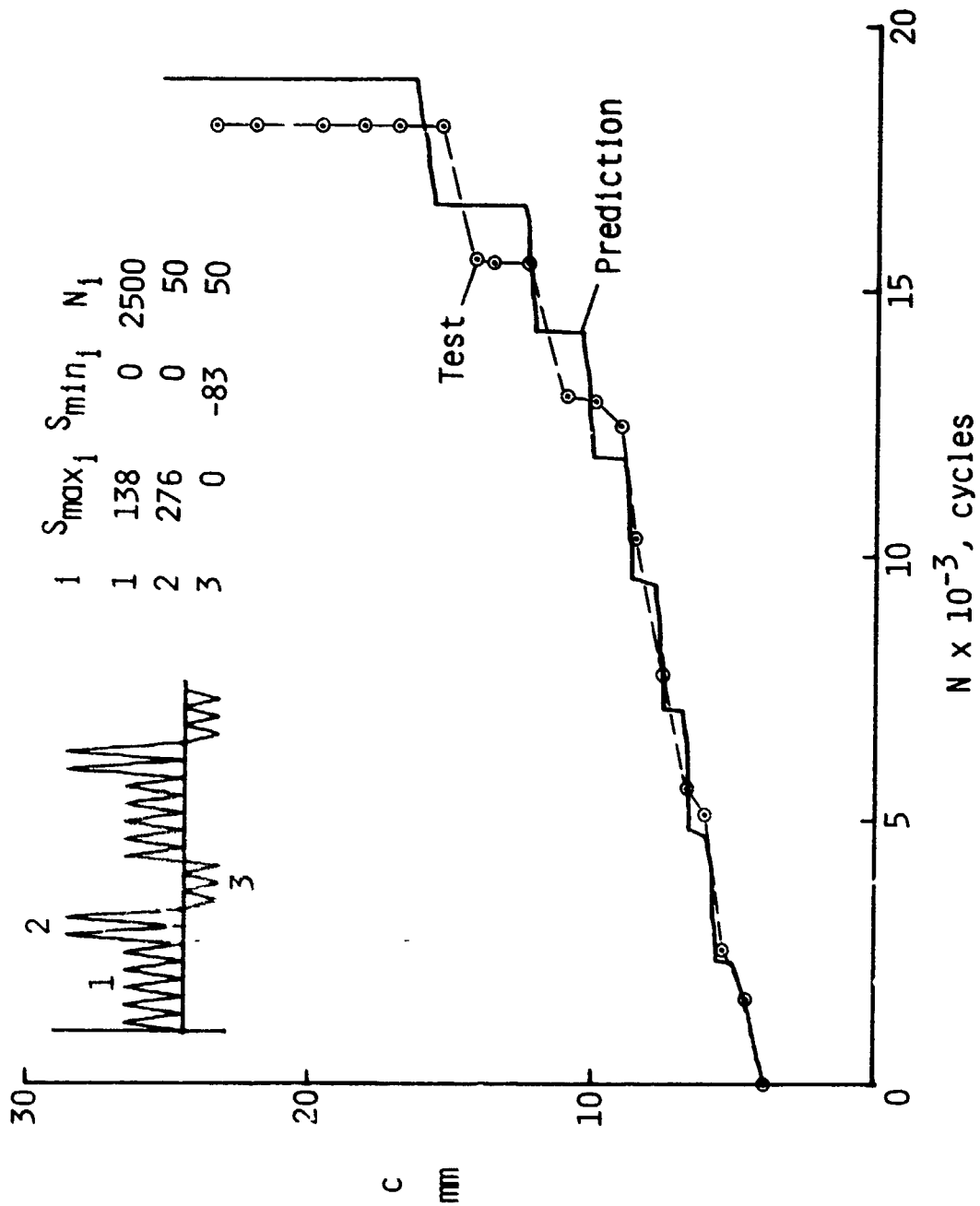


FIG. 12 - Comparison of experimental [14] and predicted crack-length-against-cycles curves during repeated block loading.

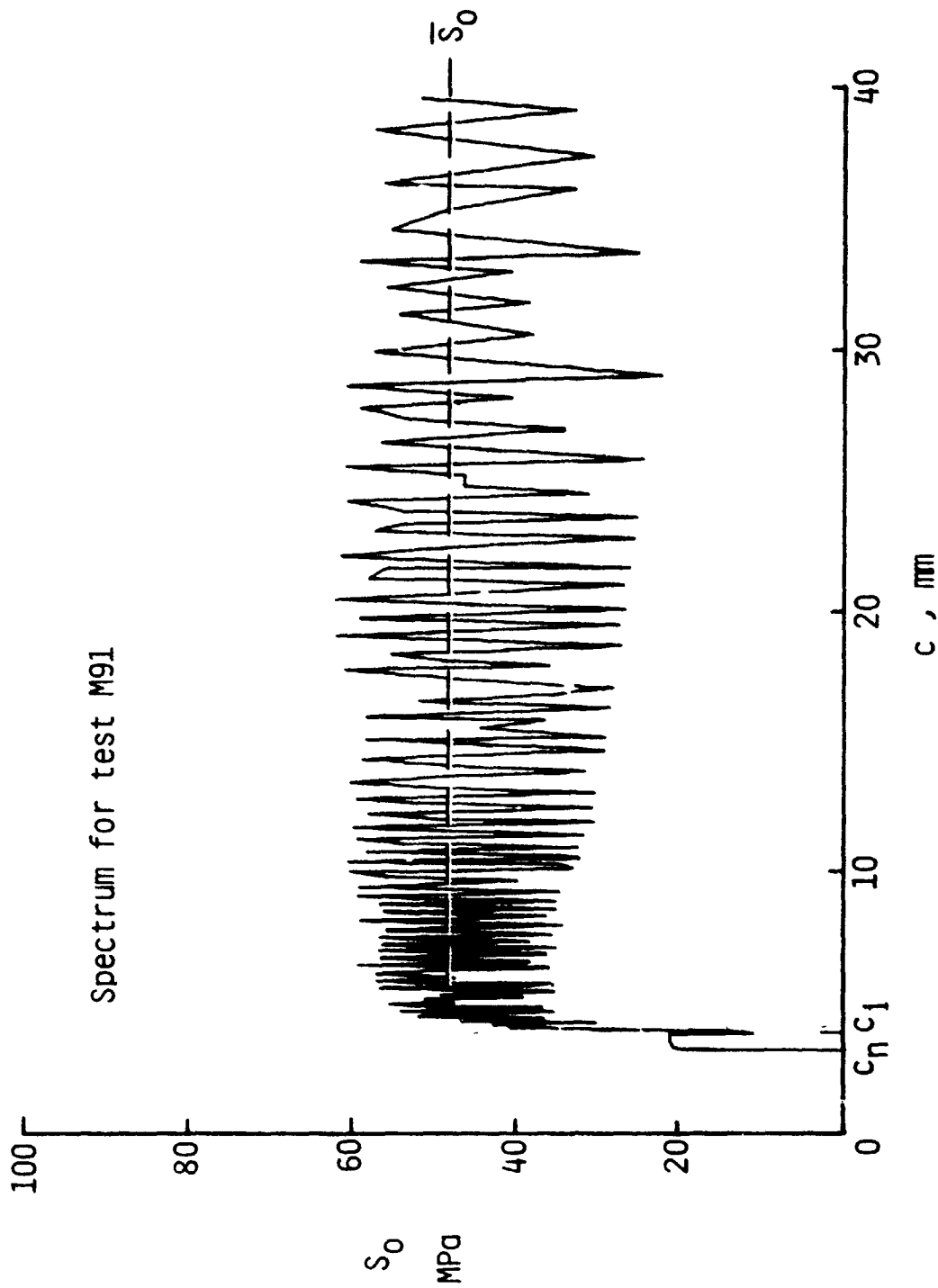


FIG. 13 - Calculated crack-opening stresses as a function of crack length under typical aircraft spectrum loading.

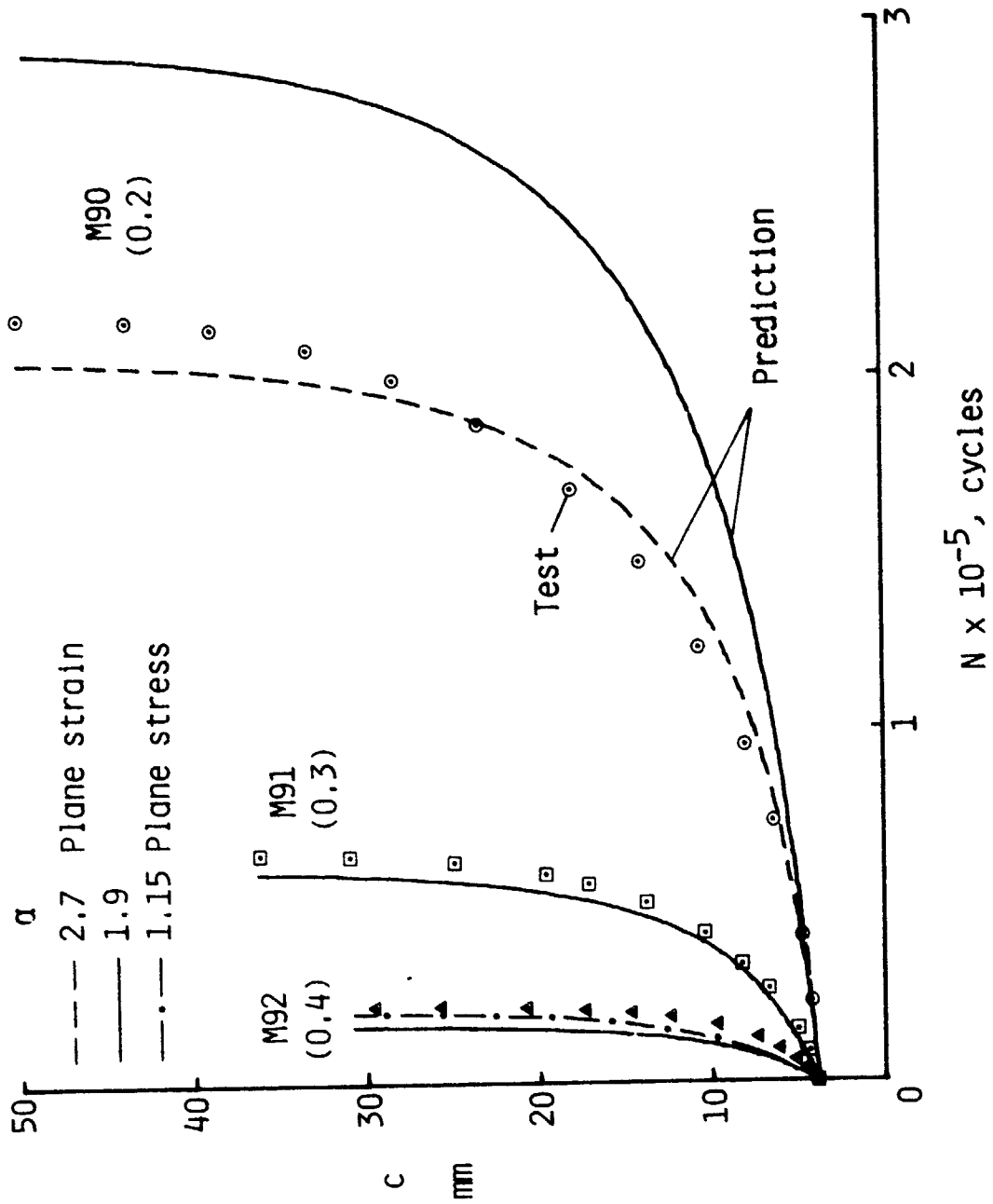


FIG. 14 - Comparison of experimental [14] and predicted crack-length-against-cycles curves for spectrum loading.

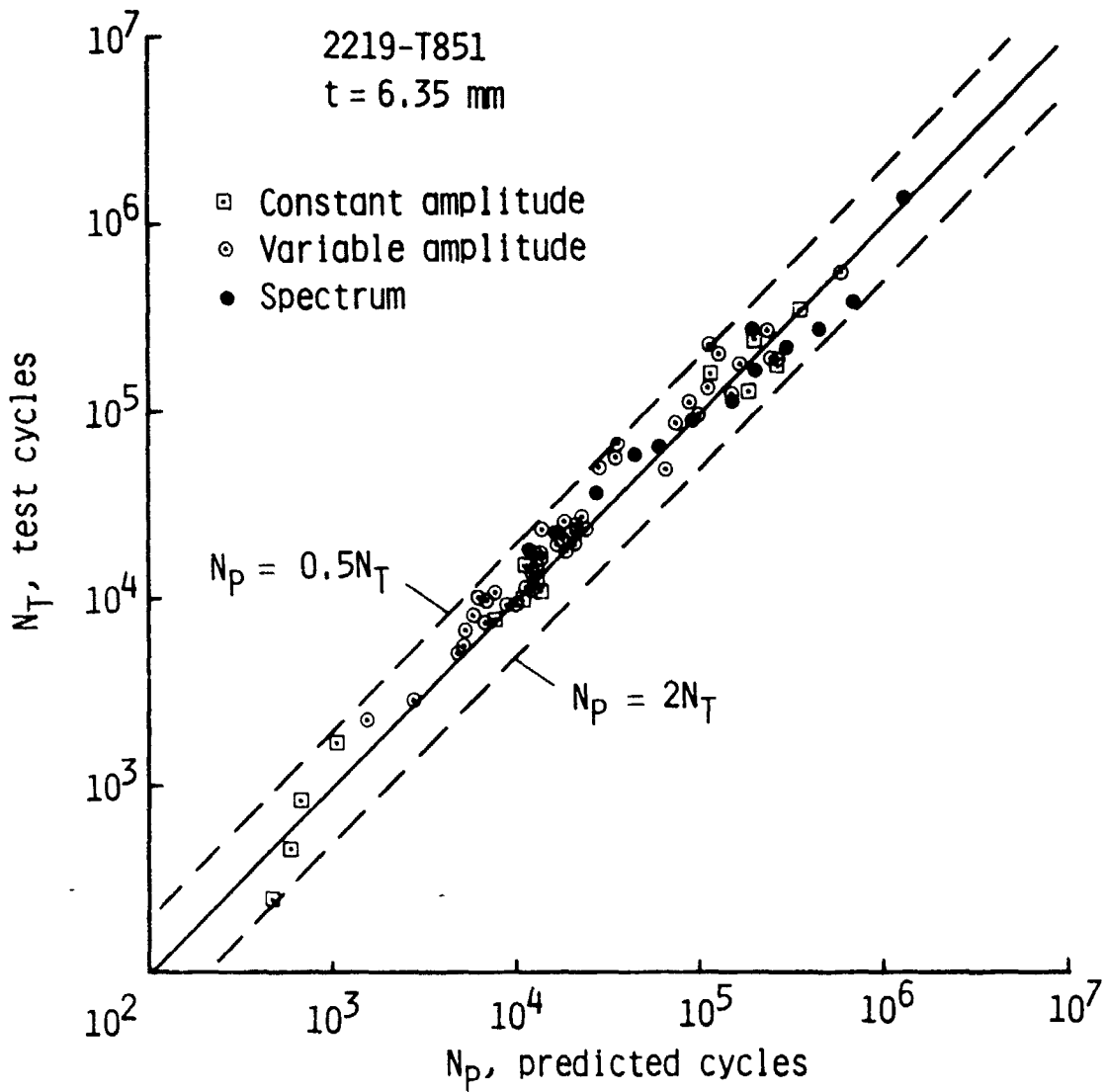


FIG. 15 - Comparison of experimental [14] and predicted cycles to failure for 2219-T851 aluminum alloy material under constant-amplitude, variable-amplitude, and spectrum loading.